Shear acoustic waves polarized along the ridged surface of an isotropic solid plate: Mode coupling effects due to the shape profile

Tony Valier-Brasier,[a] Catherine Potel,[a] and Michel Bruneau
Laboratoire d'Acoustique de l'Université du Maine (LAUM), UMR CNRS 6613, 72085 Le Mans, France and Fédération Acoustique du Nord-Ouest (FANO), FR CNRS 3110, France

(Received 15 February 2010; accepted 3 August 2010; published online 12 October 2010)

The aim of the paper is to describe the modes coupling due to scattering on small one-dimensional irregularities (parallel ridges) of the surface of isotropic solid plates, when shear horizontal waves (SH-waves) polarized along the ridges propagate perpendicularly to them. In a previous paper [Valier-Brasier *et al.*, Appl. Phys. Lett. **93**, 164101 (2008)], an analytical model was presented for describing the roughness by inertia of "teeth" which bound the ridges, through an impedancelike boundary condition, whatever shape of the roughness is. In the present paper, this shape is accounted for through a more sophisticated model, used previously for describing the effects of the roughness of walls on acoustic pressure fields in fluid-filled waveguides [Valier-Brasier *et al.*, J. Appl. Phys. **106**, 034913 (2009)], and adapted here in order to describe the modes coupling due to the scattering of these SH-waves. Moreover, the effect of a spatial periodicity of the ridges on the modes coupling is discussed, emphasizing the role played by the phase-matching (phonon relationship). Finally, comparison between both models ("teeth inertial" and "shape profile" models) is given and discussed. © *2010 American Institute of Physics*. [doi:10.1063/1.3486020]

I. INTRODUCTION

As previously mentioned (see Refs. 1 and 2, and references contained therein), the characterization of the roughness of the surface of solid plates is the subject of studies presented in the literature.[3–9] In specific applications (such as the characterization of the roughness before applying adhesive joints), the attenuation of Lamb waves when propagating along the plate is a feature that becomes relevant whenever there are distributed small irregularities of the surface of the plate which must be characterized. The incident displacement field undergoes scattering on these irregularities, which therefore induces modes coupling inside the plate.

These phenomena have been modeled using an impedance-like boundary condition for describing the effect of the roughness.[1] In this model, the corrugations (ridges) are assumed to be small deviations from the regularly shaped surface of the inner plate (bounded outwardly by the ridges). These deviations are called "small teeth" and their effects are described by their inertia. This inertia is accounted for by nonhomogeneous reactive surfaces represented by a local impedancelike operator in the frequency domain (note that the equivalent modeling for a fluid-filled, rough waveguide involves the compressibility of small cavities). The solutions are given in the frame of a modal theory, using a set of the Neumann eigenmodes of the regularly shaped surface that bounds inwardly the perturbed surface of the plate.

This previous model (called here "teeth inertial" model) is a viable tool to give a first approach for the characterization of the kind of irregularities mentioned above (small deviations), whereas the model presented in the present paper (called "shape profile" model) is a convenient tool to tackle the effects of the shape profile of the ridges (including the depth and the slope). In this approach, the displacement field of shear horizontal waves (SH-waves) is obtained from the coupling between Neumann modes of the regularly shaped surface of a waveguide that bounds outwardly the perturbed surface of the considered plate (i.e., on outer side of the perturbed surface). In many respects, the model used herein to account for the shape of the ridges (Sec. II) is an extension to the solid isotropic plate of the method used previously for describing the acoustic coupling in fluid-filled rough waveguides (presented and compared with a previous one in Refs. 2 and 10). It relies on an analytic technique, using Green's theorem and a perturbation method in the frame of the modal analysis mentioned above (i.e., using a unique set of Neumann eigenmodes of the regularly shaped surface that bounds outwardly the perturbed surface of the plate).

The comparison between both models (teeth inertial and shape profile models) is discussed, and the effects of phase-matching (phonon relationship) between spatial periods of the ridges and the spatial characteristics (namely wavenumbers along the axis of the plate) of the incident modes and the modes created by the scattering on the rough surfaces are presented (Sec. III). Finally, the approach herein built permits to highlight the effects of spatial periodicity of the ridges, using Fourier analysis to give analytically phase-matched relationships (phonon relationships) not provided yet in the frame of this modeling (Sec. IV).

II. THE FUNDAMENTAL PROBLEM

A. The plate and its boundaries

The set-up considered is a two-dimensional (2D) (x,z), homogeneous solid plate in vacuum, assumed to be infinite in the y-direction, bounded by two parallel surfaces perpen-

[a]Electronic addresses: catherine.potel@univ-lemans.fr and tony.valier-brasier.etu@univ-lemans.fr.

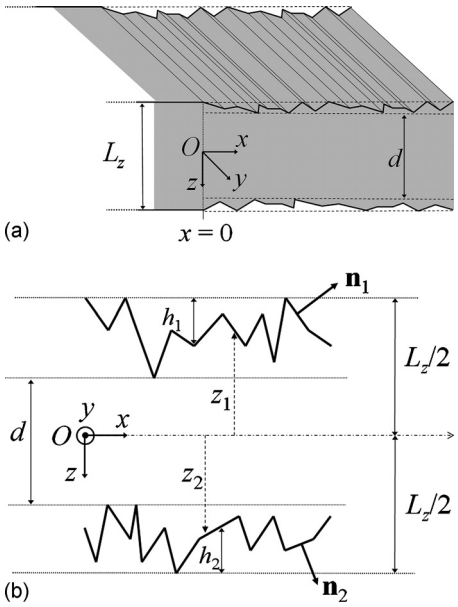

FIG. 1. Sketch of the 2D waveguide with surfaces having small deviations from the regular shape. (a) General view and (b) zoom on the corrugation.

dicular to the z-axis and having one-dimensional (1D) shape perturbation (small ridges parallel to the y-axis) (Fig. 1), the solid being characterized by its density ρ and its shear second Lamé coefficient μ. The ridged surfaces are set, respectively, at the coordinates z_1 and z_2 (which depend on the coordinate x) and their shape is defined by the local unit vectors $\mathbf{n}_1$ and $\mathbf{n}_2$ normal to the real surfaces of the plate. They are assumed to be small deviations from the regularly shaped surfaces (set at $\pm L_z/2$) bounding outwardly the perturbed surfaces. The small distance between both surfaces (the regular one and the corrugated one) are denoted $h_1 = (L_z/2)+z_1$ and $h_2=(L_z/2)-z_2$. An inner plate with regularly shaped surfaces $z=\pm d/2$ is defined as being surrounded by the 1D corrugation.

B. The basic equations

An harmonic [with a time factor $\exp(i\omega t)$], incident propagating SH-wave coming from $x\to-\infty$ is characterized by its amplitude (depending on the coordinate z) at the entrance $x=0$ of the ridged plate [domain D, $x\in(0,\infty)$, $z\in(z_1,z_2)$]. The shear displacement field, assumed to be polarized along the y-axis (along the ridges), is denoted

$$\hat{\mathbf{u}}(x,z;t)=\hat{U}_y(x,z)\exp(i\omega t)\mathbf{e}_y, \tag{1a}$$

where $\mathbf{e}_y$ denotes the unit vector that have the positive direction of the y-coordinate.

Its behavior is governed by the set of equations, including the propagation equation and the boundary conditions, which takes the following form:

$$(\partial_{xx}^2+\partial_{zz}^2+k_T^2)\hat{U}_y(x,z)=-\hat{f}(z)\delta(x), \quad \forall\,(x,z)\in D, \tag{1b}$$

$$\mathbf{T}(x,z)\,.\,\mathbf{n}_1=\mathbf{0}, \quad \forall\,x\in(0,\infty), \quad z=z_1, \tag{1c}$$

$$\mathbf{T}(x,z)\,.\,\mathbf{n}_2=\mathbf{0}, \quad \forall\,x\in(0,\infty), \quad z=z_2, \tag{1d}$$

where $k_T=\omega/c_T$, $c_T=\sqrt{\mu/\rho}$ being the speed of the shear waves in the homogeneous solid plate, where $\hat{f}(z)$ represents the source strength at $x=0$ [$\delta(x)$ being the Dirac function], and where $\mathbf{T}(x,z)$ represents the stress tensor.

The boundary conditions (1c) and (1d) on the ridged surfaces z_q $(q=1,2)$ of the real waveguide take the following form:

$$\mathbf{T}(x,z_q)\,.\,\mathbf{n}_q=[1+(\partial_x h_q)^2]^{-1/2}[T_{xy}(x,z)(\partial_x h_q) + (-1)^q T_{zy}(x,z)]\mathbf{e}_y=\mathbf{0}, \quad \forall\,x,\ q=1,2, \tag{2}$$

where

$$\mathbf{n}_q=[1+(\partial_x h_q)^2]^{-1/2}[\mathbf{e}_x(\partial_x h_q)+(-1)^q\mathbf{e}_z], \tag{3}$$

denotes the local unit vectors normal to the surfaces of the real plate, outwardly directed.

Hence, invoking the Hooke's law and accounting for the polarization along the y-axis of the SH-wave, these boundary conditions imply

$$\partial_{n_q}\hat{U}_y(x,z_q)=0, \quad \forall\,x,\ q=1,2, \tag{4a}$$

where $\partial_{n_q}=\mathbf{n}_q\cdot\nabla$ is the normal derivative with respect to the outward normal $\mathbf{n}_q$, namely:

$$\partial_{n_q}=[1+(\partial_x h_q)^2]^{-1/2}[(\partial_x h_q)\partial_x+(-1)^q\partial_{z_q}], \ q=1,2. \tag{4b}$$

The solution will be expressed (through an integral formulation, see Sec. II C) in the frame of a modal approach, using a unique set of 1D orthogonal, normalized, respectively, antisymmetrical ($\sigma=1$) and symmetrical ($\sigma=2$) eigenfunctions $\psi_m^{(\sigma)}(z)$ (with associated eigenvalues $k_m^{(\sigma)}$) of the 2D waveguide bounded by the regularly shaped, parallel, and plane surfaces set at $z=\pm L_z/2$ on the outer side of the perturbed surfaces. These eigenfunctions are solutions of the homogeneous Helmholtz equation subject to Neumann boundary conditions, in the domain $D_0=[x\in(0,\infty),\ z\in(-L_z/2,L_z/2)]$, given by $(m=0,1,2,\ldots)$

$$\begin{cases}\{\partial_{zz}^2+[k_m^{(\sigma)}]^2\}\psi_m^{(\sigma)}(z)=0, & z\in(-L_z/2,L_z/2), \quad (5a)\\ \partial_z\psi_m^{(\sigma)}(z)=0, & z=-L_z/2 \text{ and } z=L_z/2. \quad (5b)\end{cases}$$

The eigenfunctions $\psi_m^{(\sigma)}(z)$ and the corresponding eigenvalues $k_m^{(\sigma)}$ take, respectively, the well-known following expressions:

$$\psi_m^{(1)}(z)=\sqrt{2/L_z}\,\sin[k_m^{(1)}z], \tag{6a}$$

with

$$k_m^{(1)}=(2m+1)\pi/L_z, \tag{6b}$$

and

$$\psi_m^{(2)}(z)=\sqrt{(2-\delta_{m0})/L_z}\,\cos[k_m^{(2)}z], \tag{7a}$$

with

$$k_m^{(2)}=2m\pi/L_z. \tag{7b}$$

C. The integral formulation and the iterative solution

The integral formulation of the problem stated above (1a)–(1c), which involves domains $D_0=[x\in(0,\infty),\ z\in(-L_z/2,L_z/2)]$ and $D=[x\in(0,\infty),\ z\in(z_1,z_2)]$, can be written as follows:[11]

$$\left.\begin{array}{ll}(x,z)\in(D), & \hat{U}_y(x,z)\\ (x,z)\in(D_0-D), & 0\end{array}\right\}$$
$$=\int_{z_1}^{z_2}\int_0^{+\infty}G(x,z;x',z')\hat{f}(x',z')\mathrm{d}x'\mathrm{d}z'$$
$$+\sum_{q=1,2}\int_0^{+\infty}[G(x,z;x',z')\partial_{n_q}\hat{U}_y(x',z')$$
$$-\hat{U}_y(x',z')\partial_{n_q}G(x,z;x',z')]\mathrm{d}x'. \quad (8)$$

The displacement field $\hat{U}_y(x,z)$ in the domain $(D\subset D_0)$ and the Green function $G(x,z;x',z')$ in the domain (D_0) are both expressed as an expansion on the Neumann eigenfunctions $\psi_m^{(\sigma)}(z)$, namely:

$$\hat{U}_y(x,z)=\sum_{\sigma=1}^{2}\sum_{m=0}^{\infty}\hat{A}_m^{(\sigma)}(x)\psi_m^{(\sigma)}(z), \quad (9)$$

where the coefficients $\hat{A}_m^{(\sigma)}$ are the unknowns of the problem,

$$G(x,z;x',z')=\sum_{\sigma=1}^{2}\sum_{r=0}^{\infty}[g_r^{(\sigma)}(x,x')\psi_r^{(\sigma)}(z')]\psi_r^{(\sigma)}(z), \quad (10a)$$

with

$$g_r^{(\sigma)}(x,x')=\exp[-ik_{x_r}^{(\sigma)}|x-x'|]/[2ik_{x_r}^{(\sigma)}], \quad (10b)$$

$$[k_{x_r}^{(\sigma)}]^2=k_T^2-[k_r^{(\sigma)}]^2. \quad (10c)$$

Therefore, invoking Eqs. (3), (4b), (9), and (10), Eq. (8) yields straightforwardly

$$\left.\begin{array}{ll}(x,z)\in(D), & \displaystyle\sum_{\sigma=1}^{2}\sum_{m=0}^{\infty}\hat{A}_m^{(\sigma)}(x)\psi_m^{(\sigma)}(z)\\ (x,z)\in(D_0-D), & 0\end{array}\right\}$$
$$=\sum_{\beta=1}^{2}\sum_{p=0}^{\infty}\left\{\hat{F}_p^{(\beta)}(x)+\sum_{\alpha=1}^{2}\sum_{r=0}^{\infty}\hat{H}_{rp}^{(\alpha\beta)}[\hat{A}_r^{(\alpha)}(x)]\right\}\psi_p^{(\beta)}(z), \quad (11)$$

where

$$\hat{F}_p^{(\beta)}(x)=\int_{z_1}^{z_2}[g_p^{(\beta)}(x,x')\psi_p^{(\beta)}(z')]\hat{f}(z')\mathrm{d}z', \quad (12)$$

is the source term representing the energy transfer between the source (assumed to be localized at the coordinate $x'=0$) and the mode (β,p), and where

$$\hat{H}_{rp}^{(\alpha\beta)}[\hat{A}_r^{(\alpha)}(x)]=-\sum_{q=1}^{2}\int_0^{\infty}\hat{A}_r^{(\alpha)}(x')\psi_r^{(\alpha)}(z_q')\partial_{n_q'}\psi_p^{(\beta)}(z_q')$$
$$\times g_p^{(\beta)}(x,x')\mathrm{d}x', \quad (13)$$

represents the boundary modal coupling due to the shape profile of the roughness.

Then, taking into account the orthogonality properties of the eigenfunctions, the inner product, in the interval $z\in(-L_z/2,L_z/2)$, of Eq. (11) by the eigenfunction $\psi_m^{(\sigma)}$ yields the following relationship between the unknown coefficients $\hat{A}_m^{(\sigma)}$:

$$\hat{A}_m^{(\sigma)}(x)=\hat{F}_m^{(\sigma)}(x)+\sum_{\alpha=1}^{2}\sum_{r=0}^{\infty}\{\hat{H}_{rm}^{(\alpha\sigma)}[\hat{A}_r^{(\alpha)}(x)]$$
$$+B_{rm}^{(\alpha\sigma)}(x)\hat{A}_r^{(\alpha)}(x)\}, \quad (14)$$

where (the end points z_1 and z_2 depend on the coordinate x)

$$B_{rm}^{(\alpha\sigma)}(x)=\left(\int_{-L_z/2}^{z_1}\mathrm{d}z+\int_{z_2}^{L_z/2}\mathrm{d}z\right)\psi_r^{(\alpha)}(z)\psi_m^{(\sigma)}(z), \quad (15)$$

the first term in the right hand side representing the effect of the incident field on the mode m, the second ones representing the boundary modal coupling due to the shape of the roughness, and the third one accounting for the depth of the roughness (bulk modal coupling).[2,10,12]

Using an iterative method to express the amplitude of each mode $\hat{A}_m^{(\sigma)}(x)$, which assumes that the coupling function in the right hand side of Eq. (14) is a small quantity compared to the source term $\hat{F}_m^{(\sigma)}$, thus the Nth-order solution of this Eq. (14) for $\hat{A}_m^{(\sigma)}(x)$ is written as follows:

$${}^{[N]}\hat{A}_m^{(\sigma)}={}^{(0)}\hat{A}_m^{(\sigma)}+{}^{(1)}\hat{A}_m^{(\sigma)}+\cdots+{}^{(N-1)}\hat{A}_m^{(\sigma)}+{}^{(N)}\hat{A}_m^{(\sigma)}, \quad (16)$$

where ${}^{[N]}\hat{A}_m^{(\sigma)}$ denotes the Nth-order perturbation expansion for $\hat{A}_m^{(\sigma)}$, ${}^{(0)}\hat{A}_m^{(\sigma)}$ the zero order approximation (the solution without roughness), ${}^{(1)}\hat{A}_m^{(\sigma)}$ the first order correction term, and so on.

The solution without roughness and the first order solution of Eq. (14) (Born approximation, discarding the second-order term) are, respectively, given by

$${}^{(0)}\hat{A}_m^{(\sigma)}(x)=\hat{F}_m^{(\sigma)}(x)=\exp[-ik_{x_m}^{(\sigma)}x], \quad (17a)$$

$${}^{[1]}\hat{A}_m^{(\sigma)}(x)=\hat{F}_m^{(\sigma)}(x)+\sum_{\alpha=1}^{2}\sum_{r=0}^{\infty}\{\hat{H}_{rm}^{(\alpha\sigma)}[{}^{(0)}\hat{A}_m^{(\alpha)}(x)]$$
$$+B_{rm}^{(\alpha\sigma)}(x){}^{(0)}\hat{A}_r^{(\alpha)}(x)\}, \quad (17b)$$

the Nth-order taking the following form:

$${}^{[N]}\hat{A}_m^{(\sigma)}(x)=\hat{F}_m^{(\sigma)}(x)+\sum_{\alpha=1}^{2}\sum_{r=0}^{\infty}\{\hat{H}_{rm}^{(\alpha\sigma)}[{}^{[N-1]}\hat{A}_r^{(\alpha)}(x)]$$
$$+B_{rm}^{(\alpha\sigma)}(x){}^{[N-1]}\hat{A}_r^{(\alpha)}(x)\}, \quad (17c)$$

and so on.

In the results presented below, the amplitude of each mode $\hat{A}_m^{(\sigma)}(x)$, governed by Eq. (14), is truncated to the Nth-order expansion (17c) with respect to the small surface perturbation, when the omission of the further term ${}^{(N+1)}\hat{A}_m^{(\sigma)}$ [Eq. (16)] causes everywhere (i.e., for any value of x) a relative error lower than one-thousandth of the error caused when omitting term ${}^{(N)}\hat{A}_m^{(\sigma)}$, namely when $|{}^{(N+1)}\hat{A}_m^{(\sigma)}/{}^{(N)}\hat{A}_m^{(\sigma)}|\leq 10^{-3}$.

TABLE I. Parameters used to calculate the results presented in Figs. 2, 3(a), and 3(b), where f is the frequency, d the thickness of the regularly shaped surfaces inner plate, c_T is the speed of the shear wave, and k_T the associated wavenumber, Λ the spatial wavelength of the periodic roughness, ℓ the length of the roughness, λ the acoustic wavelength, and h the height of a teeth of the sawtooth profile.

$fd/c_T=1.8$	$\Lambda/\lambda=0.72$	$k_T\ell=226.2$
$d/\Lambda=2.5$	$h/d=0.005$	$\ell/\Lambda=50$

III. RESULTS AND DISCUSSIONS

A. Comparison between the shape profile approach and the teeth inertial approach

Being concerned by the improvements provided by the present approach (shape profile approach) compared to the previous one (teeth inertial approach), several simple results, yet typical of some applications, are presented in this section.

In the first example chosen here, the roughness is assumed to be a periodically corrugated surface (regularly distributed symmetrical sawtooth profile) on one boundary. The values of the adimensional parameters used are given in Table I, where f is the frequency, d the thickness of the regularly shaped surfaces inner plate, c_T the speed of the shear waves in the homogeneous solid constituting the guide, Λ the spatial wavelength of the periodic roughness, k_T the wavenumber ($k_T=2\pi f/c_T$), ℓ the total length of the roughness, λ the acoustic wavelength, and h the depth of the roughness. The incident wave is assumed to behave as the antisymmetrical mode $(m,\sigma)=(1,1)$. Three other modes, created by couplings due to the roughness, are accounted for in the calculus: the symmetrical modes $(r,\sigma)=(0,2)$ and $(r,\sigma)=(1,2)$, and the antisymmetrical one $(r,\sigma)=(0,1)$. The driving frequency is such as the following phase-matched relationship (phonon relationship) is approximately verified:[1,2,10,13–17]

$$k_{x_{m=1}}^{(\sigma=1)}+k_{x_{r=1}}^{(\sigma=2)}-2\pi/\Lambda=0, \tag{18}$$

as shown in Fig. 2 (vertical straight line at $fd/c_T=1.8$ on the dispersion and phonon curves).

The relative amplitudes (i.e., normalized to the amplitude of the incoming mode) of the modes considered here are shown in Figs. 3(a) and 3(b) as functions of the adimensional distance from the entrance of the rough part of the waveguide k_Tx, the number of iterations being always lower than $N=6$ (more often N is lower than three).

The amplitude of the incident antisymmetrical mode $(m,\sigma)=(1,1)$ [Fig. 3(a)] decreases when this mode propagates. The symmetrical mode $(r,\sigma)=(1,2)$ [Fig. 3(b)] is created from the incoming wave (initial mode generated by a source) by the diffusion process along the corrugation. Its amplitude increases when propagating backward i.e., from the right to the left (counter-propagating wave). Its relative amplitude (i.e., normalized to the amplitude of the incident mode) is quite important because it is linked with the incoming mode by the phase-matched relationship (18).

The amplitude of the two other modes considered, the symmetrical mode $(r,\sigma)=(0,2)$ and the antisymmetrical one $(r,\sigma)=(0,1)$, are much lower than the incident mode (less than 3% of the amplitude of the incident mode) because they are not linked with any other mode by a phase-matched relationship.

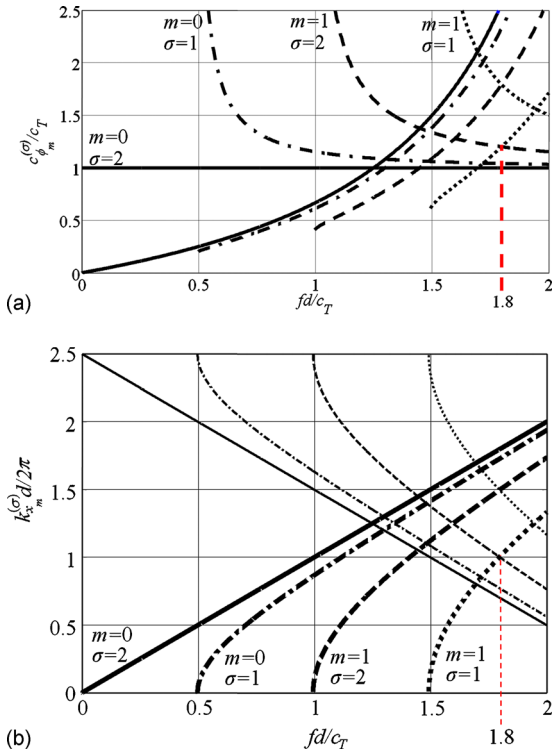

FIG. 2. (Color online) Dispersion curves (thick lines) of the guide with smooth interfaces $\{k_{x_m}^{(\sigma)}d/2\pi=\sqrt{(fd/c_T)^2-[(2m+\delta_{1\sigma})d/2L_z]^2}\}$, and curves (thin lines) corresponding to the phase-matched relation (18) $\{k_{x_m}^{(\sigma)}d/2\pi=d/\Lambda-\sqrt{(fd/c_T)^2-[(2m+\delta_{1\sigma})d/2L_z]^2}\}$, $\sigma=1$ and $\sigma=2$ corresponding, respectively, to antisymmetrical and symmetrical modes. Solid lines: mode $(m,\sigma)=(0,2)$, dashed-dotted lines: $(m,\sigma)=(0,1)$, dashed lines: $(m,\sigma)=(1,2)$, and dotted lines: $(m,\sigma)=(1,1)$. (a) Phase velocity, (b) wavenumber, as a function of the reduced frequency.

These results show several features. The attenuation of the incoming wave, and correlatively the amplitude of the symmetrical mode $(r,\sigma)=(1,2)$ created, are both more important when taking account not only the depth of the ridges but also their shape profile. As expected, these features show that the scattering process on the roughness depends not only on the depth of the roughness (teeth inertial model) but also on its slope (shape profile model), each effect contributing to the energy transfer from the incoming wave to the other modes, and then between all the existing modes.

In the second example chosen here, the roughness is assumed to be also a periodically corrugated surface (regularly distributed symmetrical trapezoidal profile) on one boundary. The values of the adimensional parameters are given in Table II. The incident wave is assumed to behave as the antisymmetrical mode $(m,\sigma)=(0,1)$. Three other modes, created by couplings due to the roughness, are accounted for in the calculus: the antisymmetrical mode $(r,\sigma)=(1,1)$, and two symmetrical modes, respectively, $(r,\sigma)=(0,2)$ and $(r,\sigma)=(1,2)$. The driving frequency is such as the following phase-matched relationships (phonon relationships) are approximately verified:

$$k_{x_{m=0}}^{(\sigma=1)}-k_{x_{r=1}}^{(\alpha=1)}-(2\pi/\Lambda)=0, \tag{19a}$$

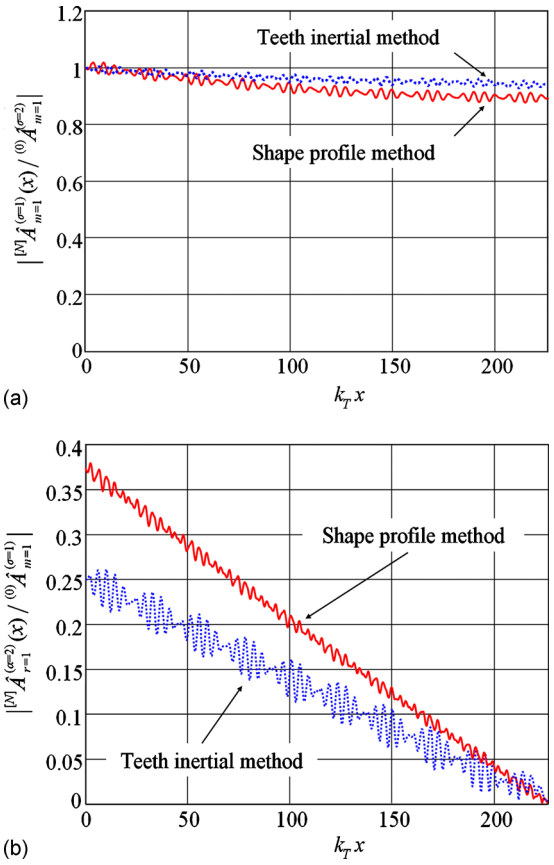

FIG. 3. (Color online) Relative amplitudes of the modes (i.e., normalized to the amplitude of the incoming mode) as functions of the adimensional distance from the entrance of the rough part of the waveguide $k_T x$, calculated using the shape profile method (solid line) and using the teeth inertial method (dashed line). (a) Incident antisymmetrical mode $(m,\sigma)=(1,1)$ and (b) symmetrical mode $(r,\sigma)=(1,2)$ satisfying the phase-matched relationship (18).

$$k_{x_{m=0}}^{(\sigma=1)} + k_{x_{r=1}}^{(\alpha=2)} - 2(2\pi/\Lambda) = 0, \tag{19b}$$

$$k_{x_{m=0}}^{(\sigma=1)} + k_{x_{r=1}}^{(\alpha=2)} - 3(2\pi/\Lambda) = 0, \tag{19c}$$

as shown in Fig. 4 (vertical straight line respectively at $fd/c_T=1.09, 1.33, 1.83$ on the dispersion and phonon curves).

The amplitude of the modes considered here are shown in Figs. 5 and 6 as functions of the adimensional distance from the entrance of the rough part of the waveguide $k_T x$, the number of iterations being always lower than $N=5$ (Fig. 5) and lower than $N=6$ (Fig. 6). Figures 5(a) and 5(b) show respectively the amplitudes of the incident antisymetrical mode $(m,\sigma)=(0,1)$ and the amplitude of the antisymmetrical mode $(r,\sigma)=(1,1)$ created by coupling for a driving frequency so that Eq. (19a) is nearly verified. Figures 6(a) and 6(b) show respectively the amplitudes of the incident antisymmetrical mode $(m,\sigma)=(0,1)$ and the amplitude of the symmetrical mode $(r,\sigma)=(1,2)$ created by coupling for a driving frequency so that Eq. (19b) is nearly verified. The amplitudes of the other modes are always much lower than the amplitude of the incoming mode because they do not obey to a phase-matched relationship at the frequencies considered here.

TABLE II. Parameters used to calculate the results presented in Figs. 4–6 where f is the frequency, d the thickness of the regularly shaped surfaces inner plate, c_T is the speed of the shear wave and k_T the associated wavenumber, Λ the spatial wavelength of the periodic roughness, ℓ the length of the roughness, λ the acoustic wavelength, and h the height of a teeth of the sawtooth profile.

$d/\Lambda=1.67$	$h/d=0.005$	$\ell/\Lambda=20$
$fd/c_T=1.09$	$\Lambda/\lambda=1.53$	$k_T\ell=192.02$
$fd/c_T=1.83$	$\Lambda/\lambda=2.56$	$k_T\ell=321.7$

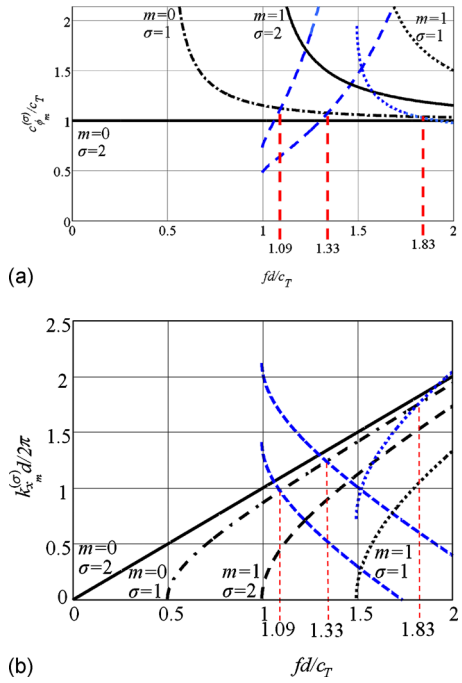

FIG. 4. (Color online) Dispersion curves (thick lines) of the guide with smooth interfaces, and curves (thin lines) corresponding to the phonon relationships (19a)–(19c), where $\sigma=1$ and $\sigma=2$ correspond, respectively, to antisymmetric and symmetric modes. Solid lines: mode $(m,\sigma)=(0,2)$, dashed-dotted lines: $(m,\sigma)=(0,1)$, dashed lines: $(m,\sigma)=(1,2)$, and dotted lines: $(m,\sigma)=(1,1)$. (a) Phase velocity and (b) wavenumber, as a function of the reduced frequency.

Note that the amplitude of the antisymmetrical mode $(r,\sigma)=(1,1)$ [Fig. 5(b)] increases when propagating forward, i.e., from the left to the right, while the amplitude of the symmetrical mode $(r,\sigma)=(1,2)$ [Fig. 6(b)] increases when propagating backward, i.e., from the right to the left.

It worth noting that the convergence of the iterative processes used to obtain the results is always improved when using the method presented here, where the integral formulation is directly substituted to the differential equations which expressed the class of problem considered (the modal solution lying on the set of eigenfunctions of the external regularly shaped plate).

B. Reflection and transmission intensity coefficients

The time average over a period of the power per unit area integrated over the thickness of the plate $\bar{\phi}$ is given by,[18]

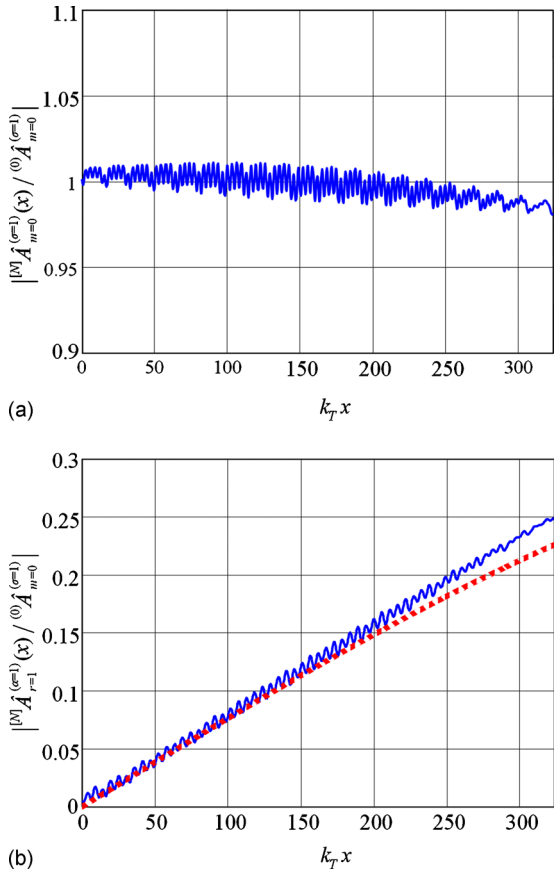

FIG. 5. (Color online) Relative amplitudes of modes (i.e., normalized to the amplitude of the incoming mode) as functions of the adimensional distance from the entrance of the rough part of the waveguide $k_T x$. (a) Relative amplitude of the incident antisymmetrical mode $(m,\sigma)=(0,1)$, (b) relative amplitude of the antisymmetrical mode $(r,\sigma)=(1,1)$ satisfying the phonon relationship (19a).

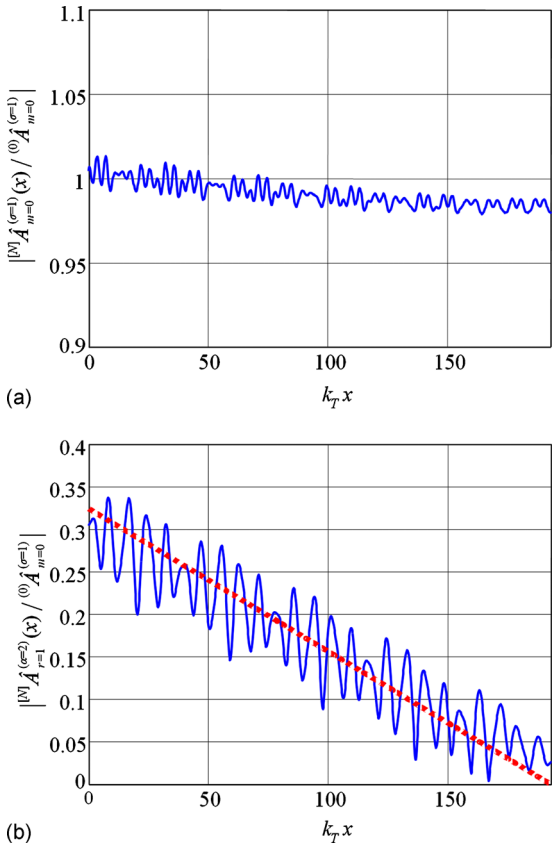

FIG. 6. (Color online) Relative amplitudes of modes (i.e., normalized to the amplitude of the incoming mode) as functions of the adimensional distance from the entrance of the rough part of the waveguide $k_T x$. (a) Relative amplitude of the incident antisymmetrical mode $(m,\sigma)=(0,1)$ and (b) relative amplitude of the symmetrical mode $(r,\sigma)=(1,2)$ satisfying the phonon relationship (19b).

$$\bar{\phi}(x)=\frac{1}{T}\int_0^T \mathrm{d}t\int_{z_1(x)}^{z_2(x)} T_{xy}\dot{u}_y \mathrm{d}z. \tag{20}$$

The modal expansion of this time averaged energy flux is found by inserting Eqs. (1a) and (9) of the velocity field $\dot{u}_y$ and the expression of the components T_{xy} of the stress tensor $\mathbf{T}$ in the integrals, and then integrating to obtain

$$\bar{\phi}(x)=-\frac{1}{4}i\omega\mu\sum_{\sigma=1}^{2}\sum_{m=0}^{\infty}\sum_{\alpha=1}^{2}\sum_{r=0}^{\infty}\{\hat{A}_m^{(\sigma)}(x)[\partial_x\hat{A}_r^{(\alpha)}(x)]^* - [\hat{A}_m^{(\sigma)}(x)]^*\partial_x\hat{A}_r^{(\alpha)}(x)\}[\delta_{\sigma\alpha}\delta_{rm}-B_{rm}^{(\alpha\sigma)}(x)], \tag{21}$$

where X^* is the complex conjugate of X.

Assuming that, at the input $x=0$ and the output $x=\ell$ of the corrugated part of the plate, the walls are regularly shaped [i.e., $z_q(0)=z_q(\ell)=(-1)^q L_z/2$, $q=1,2$] the term $B_{rm}^{(\alpha\sigma)}(x)$ vanishes, leading to

$$\bar{\phi}(x)=\sum_{\alpha=1}^{2}\sum_{r=0}^{\infty}\bar{\phi}_r^{(\alpha)}(x), \quad x=0 \text{ and } x=\ell, \tag{22}$$

where

$$\bar{\phi}_r^{(\alpha)}(x)=-\tfrac{1}{4}i\omega\mu\{\hat{A}_r^{(\alpha)}(x)[\partial_x\hat{A}_r^{(\alpha)}(x)]^* - [\hat{A}_r^{(\alpha)}(x)]^*\partial_x\hat{A}_r^{(\alpha)}(x)\}, \tag{23}$$

is the time average energy flux of each mode.

The reflection and transmission intensity coefficients are defined as

$$R_r^{(\alpha)}=|\bar{\phi}_r^{(\alpha)}(x=0)/\bar{\phi}_{inc}|, \tag{24a}$$

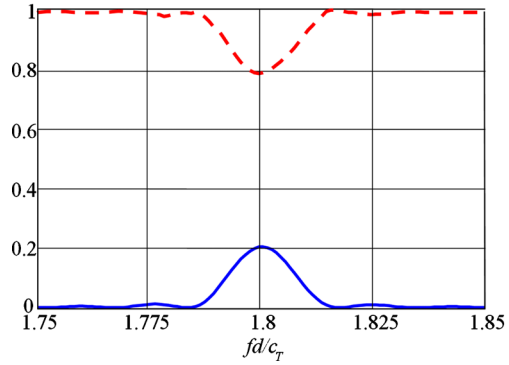

FIG. 7. (Color online) Reflection coefficient $R_{r=1}^{(\alpha=2)}$ (solid line) and transmission coefficient $T_{m=1}^{(\sigma=1)}$ (dashed line) as functions of the adimensional frequency fd/c_T.

$$T_r^{(\alpha)} = |\bar{\phi}_r^{(\alpha)}(x=\ell)/\bar{\phi}_{inc}|, \tag{24b}$$

where $\bar{\phi}_{inc}$ is the time average energy flux of the incident mode given by

$$\bar{\phi}_{inc} = \tfrac{1}{2}\omega\mu k_{x_m}^{(\sigma)}. \tag{25}$$

Hereafter, we consider the rough plate presented previously (Sec. III A).

In Fig. 7, the reflection coefficient of the symmetrical mode $(r,\sigma)=(1,2)$ $(R_{r=1}^{(\alpha=2)})$ (solid line) and the transmission coefficient of the antisymmetrical mode $(m,\sigma)=(1,1)$ $(T_{m=1}^{(\sigma=1)})$ (dashed line) are plotted [as functions of the adimensional frequency in the interval $fd/c_T \in (1.75,1.85)$]. The trends of these results obtained for SH-waves are clearly similar to those given in the literature for Lamb waves.[13]

IV. FOURIER ANALYSIS OF PERIODIC ROUGH PROFILE

It is of interest to investigate more deeply the modeling presented in this paper when applying it to periodic rough profiles (a limited but important class of roughness). As in the preceding section, the modal coupling is expressed by using the integral formulation but hereafter the shape profile is expressed as a Fourier series in order to highlight analytically the strong effects of the spatial periodicities of the roughness on the mode coupling. In the iterative method (16) used to express the amplitude of each mode $\hat{A}_m^{(\sigma)}$ (14), the first order solution $[N=1]$ is sufficient here to address these effects without loss of information, because the processes converge rapidly[2] (meaning that the results presented above are obtained mainly by the first order solution). Moreover, these trends agree with those given by Hawwa,[19] though the periodic profile is quite different.

A. Mode created by coupling (first order approximation)

Starting from Eq. (17b) to express the amplitude of a mode (r,α) created by coupling only, namely

$$\begin{aligned}{}^{(1)}\hat{A}_r^{(\alpha)}(x) = &-\sum_{q=1}^{2}\int_0^{\ell} {}^{(0)}\hat{A}_m^{(\sigma)}(x')\psi_m^{(\sigma)}(z_q)N_q^{-1}[(\partial_{x'}h_q)\partial_{x'} \\ &+(-1)^q\partial_{z_q}]\psi_r^{(\alpha)}(z_q)g_r^{(\alpha)}(x,x')\mathrm{d}x' \\ &+B_{mr}^{(\sigma\alpha)}(x)\,{}^{(0)}\hat{A}_m^{(\sigma)}(x),\end{aligned} \tag{26}$$

where the indices (m,σ) represent the incident mode (assumed to be known and unique to the lower order approximation), and assuming the following approximations, the depth of the corrugation $z_1(x)$ being much lower than the thickness of the plate L_z,

$$\psi_m^{(\sigma)}(z_1) \approx (-1)^{m+\sigma}\sqrt{(2-\delta_{\sigma 2}\delta_{m0}/L_z)}, \tag{27a}$$

$$\partial_{z_1}\psi_m^{(\sigma)}(z_1) \approx (-1)^{m+\sigma+1}\sqrt{(2-\delta_{\sigma 2}\delta_{m0}/L_z)}[k_m^{(\sigma)}]^2 h_1, \tag{27b}$$

Eq. (26), among Eqs. (10b) and (17), leads to, the incident mode (m,σ) being given,

$$\begin{aligned}{}^{(1)}\hat{A}_r^{(\alpha)}(x) = &\, i\hat{\beta}_{rm}^{(\alpha\sigma)}\int_0^{\ell}\exp[-ik_{x_m}^{(\sigma)}x'][\partial_{x'}h_1(x')]\{\partial_{x'} \\ &\times\exp[-ik_{x_r}^{(\alpha)}|x-x'|]\}\mathrm{d}x' - i\hat{\beta}_{rm}^{(\alpha\sigma)}[k_r^{(\alpha)}]^2 \\ &\times\int_0^{\ell}\exp[-ik_{x_m}^{(\sigma)}x']h_1(x')\exp[-ik_{x_r}^{(\alpha)}|x-x'|]\mathrm{d}x' \\ &+2k_{x_r}^{(\alpha)}\hat{\beta}_{rm}^{(\alpha\sigma)}h_1(x)\exp[-ik_{x_m}^{(\sigma)}x],\end{aligned} \tag{28}$$

where the term

$$\hat{\beta}_{rm}^{(\alpha\sigma)} = (-1)^{m+r+\sigma+\alpha}\frac{\sqrt{(2-\delta_{m0}\delta_{\sigma 2})(2-\delta_{r0}\delta_{\alpha 2})}}{2k_{x_r}^{(\alpha)}L_z}, \tag{29}$$

is an adimensional coupling factor.

On substituting the Fourier series of the periodic shape profile $h_1(x')$, namely

$$h_1(x') = \sum_{n=-\infty}^{+\infty}\hat{C}_n\exp\left(i\frac{2n\pi}{\Lambda}x'\right), \tag{30}$$

into Eq. (28), it follows that, for an incident mode (m,σ),

$$\begin{aligned}{}^{(1)}\hat{A}_r^{(\alpha)}(x) = &\, i\hat{\beta}_{rm}^{(\alpha\sigma)}\sum_{n=-\infty}^{+\infty}\hat{C}_n\left\{-k_{x_r}^{(\alpha)}\frac{2n\pi}{\Lambda}+[k_r^{(\alpha)}]^2\right\}\exp[-ik_{x_r}^{(\alpha)}x] \\ &\times\int_0^x\exp\left\{-i\left[k_{x_m}^{(\sigma)}-k_{x_r}^{(\alpha)}-\frac{2n\pi}{\Lambda}\right]x',\right\}\mathrm{d}x' \\ &+i\hat{\beta}_{rm}^{(\alpha\sigma)}\sum_{n=-\infty}^{+\infty}\hat{C}_n\left\{k_{x_r}^{(\alpha)}\frac{2n\pi}{\Lambda}+[k_r^{(\alpha)}]^2\right\}\exp[ik_{x_r}^{(\alpha)}x] \\ &\times\int_x^{\ell}\exp\left\{-i\left[k_{x_m}^{(\sigma)}+k_{x_r}^{(\alpha)}-\frac{2n\pi}{\Lambda}\right]x'\right\}\mathrm{d}x' \\ &+2k_{x_r}^{(\alpha)}\hat{\beta}_{rm}^{(\alpha\sigma)}\sum_{n=-\infty}^{+\infty}\hat{C}_n\exp\left\{-i\left[k_{x_m}^{(\sigma)}-\frac{2n\pi}{\Lambda}\right]x\right\}.\end{aligned} \tag{31}$$

Two kinds of phase-matching (phonon relationship) appear:

$$k_{x_m}^{(\sigma)}-k_{x_r}^{(\alpha)}-\frac{2n\pi}{\Lambda}=0, \tag{32a}$$

$$k_{x_m}^{(\sigma)}+k_{x_r}^{(\alpha)}-\frac{2n\pi}{\Lambda}=0, \tag{32b}$$

the first one representing the coupling of waves that travel in the opposite x-directions, the second one representing the coupling of waves that travel in the same x-direction.[20–23]

On one hand, if the driving frequency is such as the phonon relationship (32a) is nearly satisfied, namely if the driving frequency is such as

$$k_{x_m}^{(\sigma)}-k_{x_r}^{(\alpha)}-\frac{2n_1\pi}{\Lambda}=\varepsilon_1, \tag{33}$$

where the so-called detuning parameter ε_1 (Ref. 22) is assumed to be much lower than Λ^{-1}, then Eq. (31) of the amplitude of the mode (r,α), created by coupling with the

incident mode (m,σ), takes the following form:

$$ {}^{[1]}\hat{A}_r^{(\alpha)}(x) \approx \hat{\beta}_{rm}^{(\alpha\sigma)}\hat{C}_{n_1}\left\{k_{x_r}^{(\alpha)}\frac{2n_1\pi}{\Lambda} - [k_r^{(\alpha)}]^2\right\}\exp[-ik_{x_r}^{(\alpha)}x] \times\left[\frac{\exp(-i\varepsilon_1 x)-1}{\varepsilon_1}\right], \quad \text{if } \varepsilon_1 \neq 0, \tag{34a} $$

$$ {}^{[1]}\hat{A}_r^{(\alpha)}(x) \approx -i\hat{\beta}_{rm}^{(\alpha\sigma)}\hat{C}_{n_1}\left\{k_{x_r}^{(\alpha)}\frac{2n_1\pi}{\Lambda} - [k_r^{(\alpha)}]^2\right\}x \times\exp[-ik_{x_r}^{(\alpha)}x], \quad \text{if } \varepsilon_1 = 0, \tag{34b} $$

and then, on defining a coupling coefficient[22]

$$ {}^{n_1}\hat{\varphi}_r^{(\alpha)} = -i\hat{C}_{n_1}\left\{k_{x_r}^{(\alpha)}\frac{2n_1\pi}{\Lambda} - [k_r^{(\alpha)}]^2\right\}, \tag{35} $$

this couple of Eqs. (34a) and (34b) reduces to

$$ {}^{[1]}\hat{A}_r^{(\alpha)}(x) \approx {}^{n_1}\hat{\varphi}_r^{(\alpha)}\hat{\beta}_{rm}^{(\alpha\sigma)}x\exp\left\{-i\left[\frac{\varepsilon_1}{2}+k_{x_r}^{(\alpha)}\right]x\right\}\sin c\left(\frac{\varepsilon_1}{2}x\right). \tag{36} $$

On the other hand, if the driving frequency is such as the phonon relationship (32b) is nearly satisfied, namely if the driving frequency is such as

$$ k_{x_m}^{(\sigma)} + k_{x_r}^{(\alpha)} - \frac{2n_2\pi}{\Lambda} = \varepsilon_2, \tag{37} $$

where the detuning parameter ε_2 is assumed to be much lower than Λ^{-1}, then Eq. (31) of the amplitude of the mode (r,α), created by coupling with the incident mode (m,σ), takes the following form:

$$ {}^{[1]}\hat{A}_r^{(\alpha)}(x) \approx {}^{n_2}\hat{\xi}_r^{(\alpha)}\hat{\beta}_{rm}^{(\alpha\sigma)}(\ell-x)\exp\left\{i\left[k_{x_r}^{(\alpha)}-\frac{\varepsilon_2}{2}\right]x\right\} \times\sin c\left[\frac{\varepsilon_2}{2}(\ell-x)\right], \tag{38} $$

with (coupling coefficient)

$$ {}^{n_2}\hat{\xi}_r^{(\alpha)} = i\hat{C}_{n_2}\left\{k_{x_r}^{(\alpha)}\frac{2n_2\pi}{\Lambda} + [k_r^{(\alpha)}]^2\right\}\exp\left(-i\frac{\varepsilon_2}{2}\ell\right). \tag{39} $$

The amplitude of the antisymmetrical mode $(r,\alpha)=(1,1)$ created by coupling [Eq. (36)] is maximum for $\varepsilon_1=0$ at $x=\ell$ [Eq. (19a)] while the amplitude of the symmetrical mode $(r,\alpha)=(1,2)$ created by coupling [Eq. (38)] is maximum for $\varepsilon_2=0$ at $x=0$ [Eq. (19b)] and to a lesser extent it is maximum for $\varepsilon_3=0$ at $x=0$ [Eq. (19c)]. These amplitudes (normalized by the amplitude of the incident wave) are, respectively, shown in Figs. 8(a) and 8(b) as functions of the adimensional frequency fd/c_T (dotted lines), the full lines showing the results obtained from solving directly Eq. (14).

B. Direction of propagation: Group velocity

The group velocity can provide information, in particular, here on the direction of propagation of the modes created by coupling which can propagate either in the same direction as the incoming wave or in the opposite direction. It can be expressed for each mode (r,α) by considering the ratio of

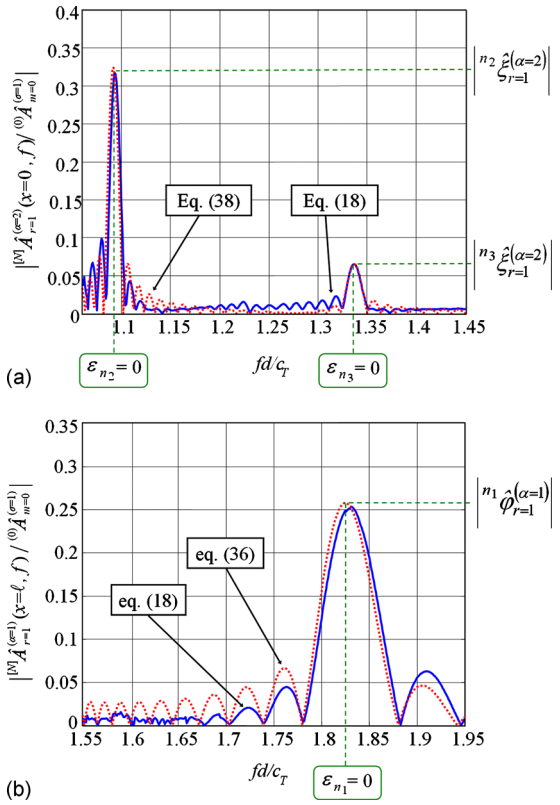

FIG. 8. (Color online) Relative amplitudes of modes (i.e., normalized to the amplitude of the incoming mode) as functions of the adimensional frequency fd/c_T. (a) Relative amplitude of the antisymmetrical mode $(r,\alpha)=(1,1)$ at $x=\ell$ satisfying the phonon relationship (32a) and (b) relative amplitude of the symmetrical mode $(r,\alpha)=(1,2)$ at point $x=0$ satisfying the phonon relationships (32b).

the time average of the energy flux $\bar{\phi}_r^{(\alpha)}$ on the time average of the total energy density (i.e., here twice the kinetic energy $\bar{K}_r^{(\alpha)}$):

$$ \bar{\phi}_r^{(\alpha)}/2\bar{K}_r^{(\alpha)}, \tag{40} $$

where the time average of the energy flux $\bar{\phi}_r^{(\alpha)}$ is given by Eqs. (22) and (23), and where the kinetic energy $\bar{K}_r^{(\alpha)}$ is given by

$$ \bar{K}_r^{(\alpha)}(x) = \frac{1}{4}\rho\omega^2\hat{A}_r^{(\alpha)}(x)[\hat{A}_r^{(\alpha)}(x)]^*, \tag{41} $$

the total kinetic being given by

$$ \bar{K}(x) = \frac{1}{T}\int_0^T dt\int_{z_1(x)}^{z_2(x)}\frac{1}{2}\rho(\dot{u}_y)^2 dz = \sum_{\alpha=1}^{2}\sum_{r=0}^{\infty}\bar{K}_r^{(\alpha)}(x). \tag{42} $$

On substituting Eq. (36) of the amplitude ${}^{[1]}\hat{A}_r^{(\alpha)}(x)$ into Eqs. (23) and (42), it is found straightforwardly that,

$$ \frac{\bar{\phi}_r^{(\alpha)}}{2\bar{K}_r^{(\alpha)}} = c_{g_r}^{(\alpha)} + \frac{c_T}{k_T}\frac{\varepsilon_1}{2}, \tag{43} $$

where $c_{g_r}^{(\alpha)}=(c_T/k_T)k_{x_r}^{(\alpha)}$ represents the group velocity of the mode (r,α) considered when the phonon relationship (33) is assumed.

Equation (43) shows that this mode, shown in Fig. 5(b) propagates forwardly, i.e., in the same direction as the incoming wave ($c_{g_r}^{(\alpha)} > 0$).

Similarly, on substituting Eq. (38) of the amplitude ${}^{[1]}\hat{A}_r^{(\alpha)}(x)$ into Eqs. (23) and (42), it is found straightforwardly that,

$$\frac{\bar{\Phi}_r^{(\alpha)}}{2\bar{K}_r^{(\alpha)}} = -c_{g_r}^{(\alpha)} + \frac{c_T}{k_T}\frac{\varepsilon_2}{2}, \tag{44}$$

which shows that this mode, shown in Fig. 6(b), propagates backwardly (opposite to the direction of the incoming wave as mentioned in Sec. III A).

V. CONCLUSIONS

In conclusion, it can be noted that a major advantage of the method used here to express the effect of the roughness on SH-waves, in comparison with previous methods such as those presented in Refs. 1, 2, 10, and 11, is that it does not require lengthy calculations to obtain the coupling effects of the nonlocalized perturbation. Basically, this method is completely general when assuming however small perturbations (small depths and small slopes). Therefore, the method can be straightforwardly extended to any shape of roughness and even to more sophisticated lamb waves (subject to modifying the basic expansions and to accounting for the coupling between longitudinal and transversal waves). Moreover, it is worth noting that, owing to SH-waves in plates behave similarly to torsional waves in circular pipes, the results obtained for the first ones can be extended to the second ones (this can be of interest in practical pipe testing).

ACKNOWLEDGMENTS

Support from CNRS through the research group GDR-2501 is gratefully acknowledged. The authors also want to thank their colleagues in the "Fédération d'Acoustique du Nord Ouest" (FANO, FR CNRS 3110) for their helpful discussions.

[1] T. Valier-Brasier, C. Potel, and M. Bruneau, Appl. Phys. Lett. **93**, 164101 (2008).
[2] T. Valier-Brasier, C. Potel, and M. Bruneau, J. Appl. Phys. **106**, 034913 (2009).
[3] O. I. Lobkis and D. E. Chimenti, J. Acoust. Soc. Am. **102**, 143 (1997).
[4] D. E. Chimenti and O. I. Lobkis, Ultrasonics **36**, 155 (1998).
[5] S. Banerjee and T. Kundu, J. Acoust. Soc. Am. **119**, 2006 (2006).
[6] A. Boström, J. Acoust. Soc. Am. **85**, 1549 (1989).
[7] A. El-Bahrawy, J. Sound Vib. **170**, 145 (1994).
[8] T. Kundu, S. Banerjee, and K. V. Jata, J. Acoust. Soc. Am. **120**, 1217 (2006).
[9] S. Banerjee and T. Kundu, Int. J. Solids Struct. **43**, 6551 (2006).
[10] C. Potel and M. Bruneau, J. Sound Vib. **313**, 738 (2008).
[11] M. Bruneau and T. Scelo, *Fundamentals of Acoustics* (ISTE, UK, 2006).
[12] K. S. Sum and J. Pan, J. Acoust. Soc. Am. **119**, 2201 (2006).
[13] M. Bavencoffe, A. Hladky-Hennion, B. Morvan, and J. Izbicki, IEEE Trans. Ultrason. Ferroelectr. Freq. Control **56**, 1960 (2009).
[14] D. Leduc, A.-C. Hladky, B. Morvan, J.-L. Izbicki, and P. Pareige, J. Acoust. Soc. Am. **118**, 2234 (2005).
[15] B. Morvan, A.-C. Hladky-Hennion, D. Leduc, and J. L. Izbicki, J. Appl. Phys. **101**, 114906 (2007).
[16] C. Potel, D. Leduc, B. Morvan, C. Depollier, A.-C. Hladky-Hennion, J. L. Izbicki, P. Pareige, and M. Bruneau, J. Appl. Phys. **104**, 074908 (2008).
[17] C. Potel, D. Leduc, B. Morvan, C. Depollier, A.-C. Hladky-Hennion, J. L. Izbicki, P. Pareige, and M. Bruneau, J. Appl. Phys. **104**, 074909 (2008).
[18] J. Achenbach, *Wave Propagation in Elastic Solids* (North Holland, Amsterdam, 1987).
[19] M. A. Hawwa, J. Acoust. Soc. Am. **102**, 137 (1997).
[20] C. Elachi and C. Yeh, J. Appl. Phys. **45**, 3494 (1974).
[21] L. Brillouin, *Wave Propagation in Periodic Structures* (Dover, New York, 1953).
[22] D. Royer and E. Dieulesaint, *Elastic Waves in Solids: Generation, Acousto-Optic Interaction, Applications* (Springer, Paris, 2000).
[23] S. R. Seshadri, J. Appl. Phys. **63**, R115 (1988).